Nuclear Inst. and Methods in Physics Research, A 880 (2018) 75–79

Contents lists available at ScienceDirect

Nuclear Inst. and Methods in Physics Research, A

journal homepage: www.elsevier.com/locate/nima

Measurement of thick target neutron yield from the reaction (p + ^{181}Ta) with projectiles in the range of 6–20 MeV

Sabyasachi Paul [a,b], G.S. Sahoo [a,b], S.P. Tripathy [a,b,*], S.C. Sharma [c], D.S. Joshi [a], T. Bandyopadhyay [a,b]

[a] Health Physics Division, Bhabha Atomic Research Centre, Mumbai - 400085, India
[b] Homi Bhabha National Institute, Anushaktinagar, Mumbai - 400 094, India
[c] Nuclear Physics Division, Bhabha Atomic Research Centre, Mumbai - 400085, India

ARTICLE INFO

Keywords:
Neutron spectral yield
Proton on Ta
CR-39
autoTRAK_n

ABSTRACT

^{181}Ta is a commonly used backing material for many targets in nuclear reaction studies. When the target thickness is less than the range of bombarded projectiles, the interaction via Ta(p,n) reactions in the backing can be a significant source of background. In this study, the neutron spectral yields from the reaction of protons of different energies (between 6 to 20 MeV) with a thick Ta target were determined using CR-39 detectors. The results from this study can be used as a correction factor in such situations. The parameters of registered tracks in CR-39 were analysed using an in-house image analysing program autoTRAK_n and then to derive the associated dose values. The spectral yields obtained experimentally were compared with those obtained from the theoretical calculations. The neutron yield was found to increase with increase in projectile energy mainly due to the opening of reaction channels from (p, n) to (p, 3n).

1. Introduction

The knowledge of reactions induced by fast neutron beams has acquired attention since the advent of accelerators capable of delivering high current beams in the intermediate energy regime. The measurement of total yield and energy distribution of neutrons generated by bombarding light ions on a thick target is important for many nuclear reaction studies, therapy applications and radiation protection purposes [1–4]. The extended attention is further required for shielding calculations where the source term needs to be defined accurately. Keeping this in mind, an attempt has been made in this study to measure the neutron spectra from a commonly used target material in accelerator environment, i.e. ^{181}Ta.

Ta has plenty of applications in accelerator environments such as beam dump, target holder, etc. From the radiological point of view, the neutrons produced by bombarding 6–20 MeV protons on a Ta target is important due to the opening of multiple reaction channels, viz. (p, n), (p, 2n) and (p, 3n). Emission of other charged particles was considered to be negligible due to very low production cross sections and relatively higher Coulomb barrier with respect to the effective compound nuclear excitations.

Measurements were made with 8 different projectile energies (6–20 MeV with a gap of 2 MeV). These energies were categorically chosen to study the effect of different reaction channels on the spectral yield. The first 2 energies (6, 8 MeV proton) correspond to (p, n) reaction solely, next 4 energies (10, 12, 14, 16 MeV) to both (p, n) and (p, 2n) and last two energies (18, 20 MeV) open up all three reaction channels ((p, xn) (x = 1–3)). The neutron spectra were obtained from the measured tracks in CR-39. A specially developed image analysing program (autoTRAK_n) [5–8] was used to generate the neutron spectra from the distribution of tracks and then to estimate the dose equivalent by folding the spectra with dose conversion coefficients. Though several methods (e.g. time of flight [9,10], activation foils [11,12], Bonner sphere spectrometry [13,14], etc.) are commonly being used to measure the neutron spectra, there are certain advantages of using CR-39 for this purpose. Considering accelerator radiation environment, the exposure of CR-39 to the generated neutrons consumes much less time and space, no sensitivity to low LET particles such as gamma and X-rays, no RF interferences [15,16]. Furthermore, these detectors have an excellent charge particle registration capability in time integral mode, which makes it suitable specially in a pulsed radiation field [17–19].

* Corresponding author at: Health Physics Division, Bhabha Atomic Research Centre, Mumbai - 400085, India.
E-mail address: tripathy@barc.gov.in (S.P. Tripathy).

https://doi.org/10.1016/j.nima.2017.10.046
Received 16 September 2017; Accepted 17 October 2017
Available online 3 November 2017
0168-9002/

Furthermore, due to small dimensions it is convenient to irradiate at any location which also eliminates the problem of angular resolution, compared to the conventional measurement techniques involving large size neutron detectors.

2. Materials and methods

2.1. Irradiation

The CR-39 detectors ($12\times12\times1.5$ mm^3) were irradiated with 8 different proton energies ranging between 6 to 20 MeV on a thick Ta plate (3.5 mm) in the 6 m facility of BARC-TIFR Pelletron accelerator facility where the proton fluence was found to be maximum. The irradiation set up [8] had a Ta collimator of 4 mm diameter through which the protons were directed to interact with the 3.5 mm thick Ta disk. The target thickness was so chosen that the projectiles were completely stopped within the target, making measurements feasible at the extreme forward angle with respect to the beam direction. The detectors were placed below the target plate, normal to the direction of projectiles. All the irradiations were carried out with a beam current of 70 nA at 0° with respect to the beam direction. The total fluence of protons falling on the target was about $(1.58\ \pm0.03)\times10^{15}$. The proton current was measured through a charge integrator connected to Faraday cup. The maximum penetration depth considering the 20 MeV (maximum energy used in this study) protons were calculated using the SRIM code [20] and was found to have a range of 0.6 mm in Ta, eliminating the possibility of direct proton interaction with the detector. The neutrons generated from these interactions (protons on Ta) were then registered in the CR-39 detectors which were developed by suitable etching procedures followed by imaging and measurement of track parameters. A pristine detector was also used in the experimental environment for background correction.

2.2. Track development and imaging

The detectors after irradiation were subjected to the conventional chemical etching technique (6.25 N NaOH at 70 °C for 6 h) for the development of tracks. The developed tracks were viewed under an optical microscope (Carl-Zeiss) in transmission mode. The 2-dimensional track images were captured with a 5 MP camera attached to it. The transmitted light is adjusted such that the luminosity at the centre of the tracks remains higher compared to the boundary edges. The depth profile of each track in the CR-39 detector due to normal and angular incidence of the recoil protons were determined using an in-house autoTRAK_n program [3–6] based on the grey level variations in and around each track.

2.3. Generation of neutron spectra

The track depth distribution was then folded with energy dependent track to neutron response function [21] to generate the neutron spectra. The spectra were then bin-wise multiplied with the neutron dose conversion coefficients adopted from ICRP-74 [22] to obtain the dose equivalent. After complete analysis, the neutron spectra and total yield were computed per unit charge for different proton energies. The background correction was carried out using a pristine detector processed with the similar procedures.

3. Results and discussion

The neutron yields from experiment were compared with those obtained from theoretical calculations for all the projectile energies used in this study, which is described below.

3.1. Theoretical estimation of the neutron yield

In the present study, energy of protons was varied from 6 to 20 MeV, leading to the progressive opening of Ta (p, n) to Ta (p, 3n) reactions with increasing energy. Registration of other charged particles in CR-39 detector were neglected considering sufficiently thick Ta disk used in the experimental setup and nominal production of the charged particles within the reaction volume due to large Coulomb barrier.

The generated neutrons passing through the target material reaches the CR-39 detector after continuous degradation in energy because of attenuation within the target material. The effective range of the proton energies at the target will lie between the incident projectile energy to neutron emission threshold of the compound nucleus. So, the possible neutron energies can vary from zero to a maximum projectile energy depending on the Q-value of the reaction. To solve this varying energy range of projectiles, a differential thick target neutron yield (TTNY) estimation was carried out in this work. To reduce the computational load, the continuous degradation of energy has been assumed to be occurring in a quantum of small energy intervals ΔE (considered as 1 MeV for the present study). Accordingly, the corresponding target slab thickness was calculated. It was assumed that within this target thickness, all particles have interacted with the target material with an average projectile energy $\left(\overline{E}_p\right)$. Finally, the emitted spectra from all these slabs are summed up to obtain the final neutron spectra. During this process of calculations, the energy straggling of the projectile and multiple scatterings were not considered [23]. The theoretical estimation of the total number of emitted neutrons for a specific proton energy per unit charge, were estimated using the following parameters at each ith thin slab corresponding to unit energy decrement, viz. (i) Number of target atoms interacting with the protons within the average energy slab $\left(N_T\right)$, (ii) the stopping power of projectile in the target medium in units of MeV mg^{-1} cm^{-2}$\left(S_m\right)$, (iii) molar mass of the target material A_T, (iv) fusion cross section for compound nucleus formation $\left(\sigma\left(\overline{E}_p^i\right)\right)$, (v) the total projectile fluence (ϕ), (vi) emission cross section $\left(\sigma_{(n,xn)}\right)$ of the individual reactions (p, n), (p, 2n), (p, 3n). The estimations were carried out using the following relations.

$$N_T^i = \frac{6.023\times10^{20}}{S_m^i A_T} \tag{1}$$

$$Y\,(p,xn) = \sum_{x=1}^{x}\left\{\sum_{i=1}^{n} N_T^i \sigma_{(n,xn)}\left(\overline{E}_p^i\right)\phi \times \exp\left[-N_T\left\{\sum_{k=1}^{i-1}\sigma_{fus}\left(\overline{E}_p^k\right)x_k\right\}\right]\right\} \tag{2}$$

where, the yield calculated is for a different reactions, for this case $x = 1$, 2 and 3 for different energies and the projectile energy $\overline{E}_p^i$ incident on i-th thin slab and the average energy $\overline{E}_p^i$ at this slab is computed for the incident projectile energy E_p^0 by,

$$E_p^i = E_p^0 - (i-1)\,\Delta E$$
$$\overline{E}_p^i = \left(E_p^i + E_p^{i+1}\right)/2 \tag{3}$$

The slab thickness x_i was estimated from the stopping power of the projectile dE/dx as,

$$x_i = \int_{E_p^i}^{E_p^{i+1}} \frac{dE}{-dE/dx} \tag{4}$$

The running index n represents the number of thin slices depending upon the discrete energy decrement, $n = \left(E_p^0 - E_p^{Th}\right)/\Delta E$ where, E_p^{Th} is the projectile neutron emission threshold. The number of atoms seeing the average proton energy and energy losses are calculated using the SRIM code and the fusion cross-sections are obtained from the PACE4 [24] code. Emission cross-sections for the individual reactions are obtained from different earlier cross-section data [25–31] as shown

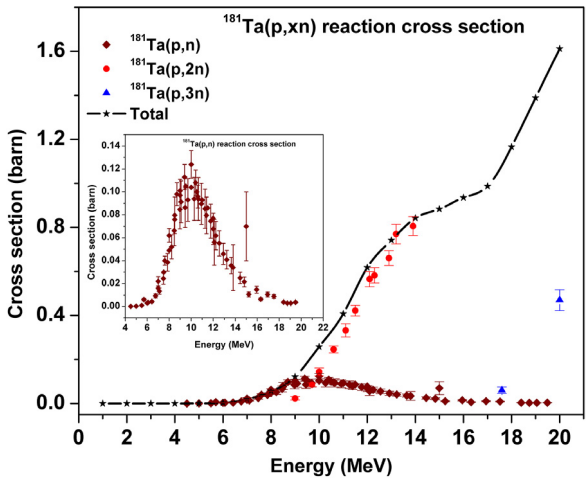

Fig. 1. Emission cross-section of different ^{181}Ta(p, xn) reaction with total cross-section in the energy range up to 20 MeV.

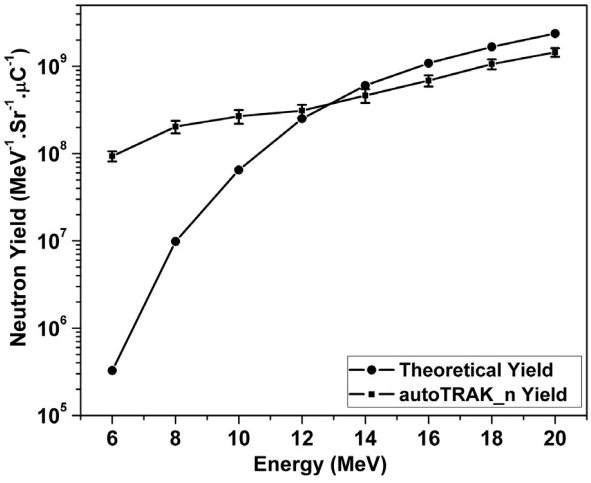

Fig. 2. Comparison of total neutron yields obtained from theoretical calculations and experimentally measured values for the projectile energies between 6–20 MeV.

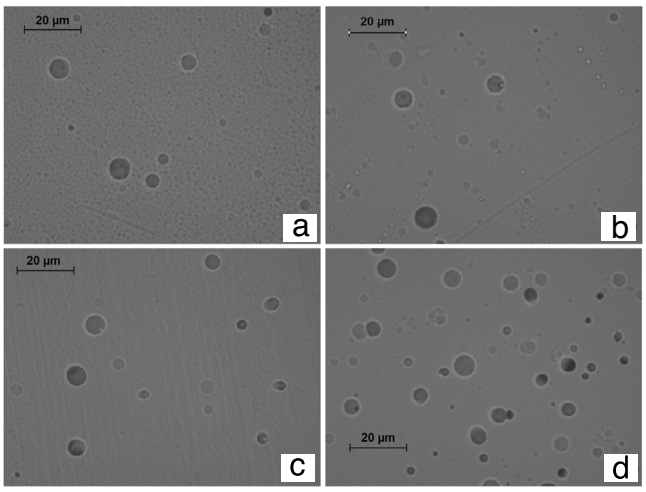

Fig. 3. The track densities at different projectile energies (a) 6 MeV; (b) 10 MeV; (c) 14 MeV and (d) 18 MeV.

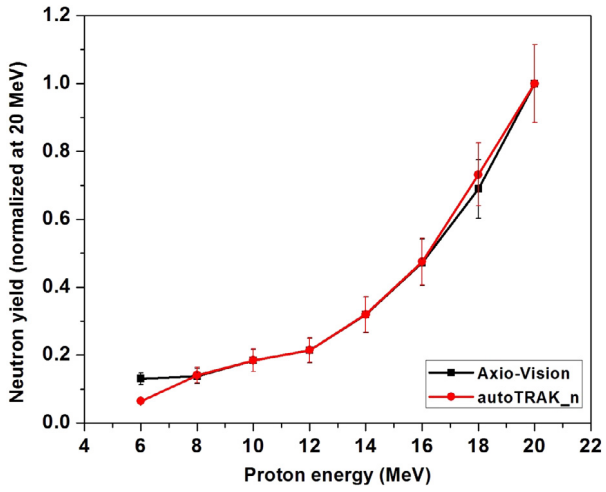

Fig. 4. Comparison of neutron yields (normalised at 20 MeV protons) obtained using Axio-Vision and autoTRAK_n programs.

in Fig. 1. The figure shows that, emission of neutrons starts only above 4 MeV of proton energy and as the energy increases, other emission channels open up. Range of proton energy used in the present study completely scans the single neutron emission process (inset figure) and rest of the channels remains partially open till 20 MeV. An interpolated energy dependence of the total cross section is shown by the black line.

Finally, the effective neutron yields for the individual reactions are estimated and these are summed over to obtain the total neutron yields for all projectile energies. The comparison between the theoretical and experimental neutron yields is shown in Fig. 2. The figure describes a good corroboration between the theoretical and measured yields above 12 MeV proton energies. At lower proton energies, the theoretically estimated neutron numbers are found to be underestimated compared to the experimental values.

3.2. Comparison of neutron yields obtained using 2 different image analysing programs (Axio-Vision and autoTRAK_n) at different proton energies

An attempt has been made in the present study to compare the total neutron yield obtained using Axio-Vision software [Carl Zeiss, Germany] with that obtained using the in-house developed autoTRAK_n program. The track density profiles at different proton energies are shown in Fig. 3 for four different energies, viz., 6, 10, 14 and 18 MeV. As can be seen in the figure, the track density was found increase with the increase in projectile energy.

In the present study, for comparison purpose, the results obtained from both the programs (autoTRAK_n and Axio-Vision) were normalised with respect to the yield at 20 MeV protons as shown in Fig. 4. This shows a good corroboration in terms of the total neutron yield. The associated uncertainty mentioned in the figures is only from the statistical fluctuations.

3.3. Analysis of neutron spectra at different proton energies

The neutron spectra obtained from the reaction ^{181}Ta(p, xn) at different proton energies are presented in Fig. 5. All the spectra were measured at 0° with respect to the projectile direction. The depth profiles of tracks were generated from the 2D track images by correlating with the grey level variations (more detail can be found in 3–5). The depths of recoil tracks were correlated with the particle range obtained from SRIM code. These were then folded with energy dependent track to neutron response function to obtain the neutron fluence within the energy bin per μC charge of incident protons.

Fig. 5(a) and (b) show an increasing neutron yield with increasing proton energy, the first one is for proton energies between 6–12 MeV

Table 1
Comparison of the neutron yields from autoTRAK_n and theoretical estimation and dose equivalent per unit projectile charge at various projectile energies.

Proton energy (MeV)	Theoretical neutron yield (μC^{-1})	autoTRAK_n neutron yield (μC^{-1})	Dose equivalent (mSv μC^{-1})
6	3.27×10^{5}	9.34×10^{7} $\pm1.23\times10^{7}$	38.79
8	9.86×10^{6}	2.04×10^{8} $\pm3.33\times10^{7}$	67.33
10	6.50×10^{7}	2.67×10^{8} $\pm4.78\times10^{7}$	99.57
12	2.51×10^{8}	3.10×10^{8} $\pm5.31\times10^{7}$	129.85
14	6.04×10^{8}	4.63×10^{8} $\pm8.23\times10^{7}$	199.14
16	1.08×10^{9}	6.88×10^{8} $\pm1.02\times10^{8}$	296.95
18	1.67×10^{9}	1.06×10^{9} $\pm1.40\times10^{8}$	460.31
20	2.37×10^{9}	1.45×10^{9} $\pm1.65\times10^{8}$	622.19

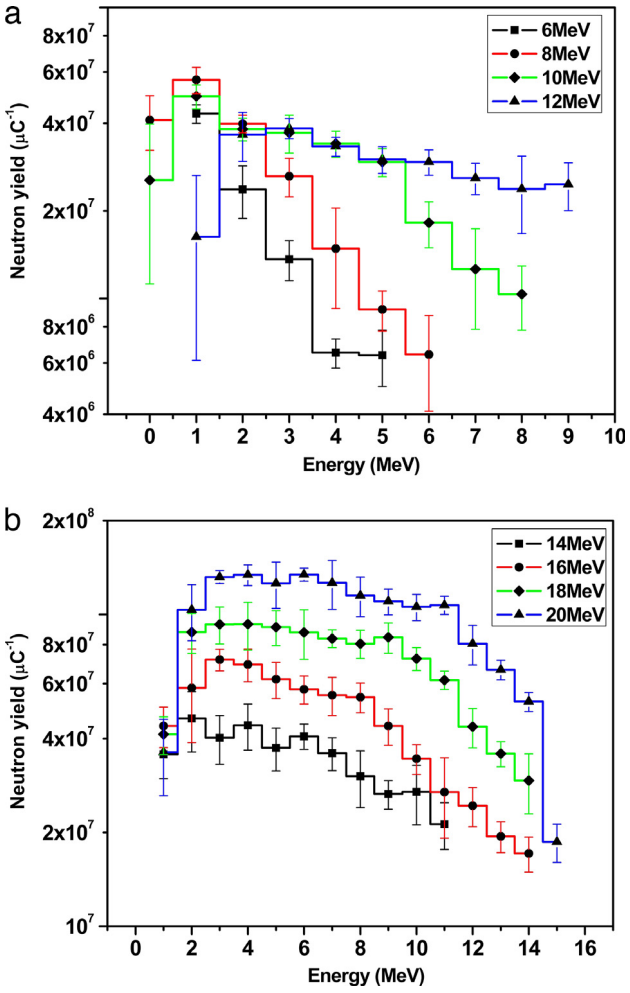

Fig. 5. Neutron spectral yield from ^{1}H + ^{181}Ta reactions measured with CR-39 detector and analysed with autoTRAK_n program, for projectile energies: (a) 6–12 MeV, (b) 14–20 MeV.

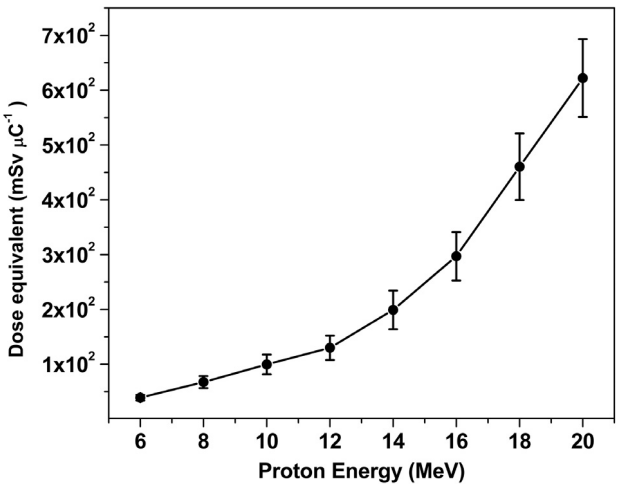

Fig. 6. Neutron dose equivalent per μC charge of protons at the energy range of 6–20 MeV for the reaction ($^{1}H+^{181}Ta$).

and the second one is for 14–20 MeV. The neutron yield measured with CR-39 detector and analysed with autoTRAK_n program were found to be between 9.34×10^{7} to 1.45×10^{9} neutrons per μC of incident proton current at 6 and 20 MeV of proton energy respectively. This progressive increase in the neutron yield is due to the opening of different reaction channels at increasing proton energies as discussed earlier. In case of 6 and 8 MeV protons, due to small nuclear excitation only Ta(p, n) reaction channel gets opened after the compound nucleus formation, as shown in Fig. 1. In Fig. 5(a), the increase in the neutron yield in case of 8 MeV compared to the 6 MeV protons is due to the increase in the emission cross-section. From 10 MeV protons, the second set of reaction channel (p, 2n) opens up thereby increasing the neutron yield till 16 MeV. After 18 MeV, (p, 3n) reaction also starts contributing in the emission leading to the larger emission of neutrons per μC of incident protons.

3.4. Estimation of the neutron dose at different proton energies

The neutron dose equivalents for these reactions were estimated using the ICRP-74 dose conversion coefficient [14] and the measured neutron spectra according to the relation

$$Dose = \sum_{i=1}^{n} \left(\phi_i \times DCC_i \times 10^{-12}\right) Sv \quad (5)$$

where, i is the energy bin index, ϕ_i and DCC_i are the corresponding neutron fluence (cm^{-2}) and ICRP-74 dose conversion coefficients (pSv cm^2) at ith energy bin. The dose equivalents due to different proton energies are given in Fig. 6, which show a progressively increasing pattern. The dose equivalent was found to be increasing gradually from about 39 mSv μC^{-1} (for 6 protons) to 622 mSv μC^{-1} (for 20 MeV protons). All these values are listed in Table 1.

4. Conclusion

In the present work, the Ta(p, xn) reactions were studied using CR-39 detectors at different proton energies starting from 6 MeV to 20 MeV. The energy range was chosen so that the effect of all three (p, xn) reactions (for x = 1–3) on the spectral yield could be analysed. The in-house autoTRAK_n image processing program was utilised to determine the neutron spectral yield per unit charge of protons. The measured thick target neutron yields were found to be in a good agreement with those of the theoretical calculations above 12 MeV. The yield pattern was also verified using another image analysing program, Axio-Vision software. The dose equivalent due to the emission neutrons were estimated from the study and were found to vary from about 39 mSv μC^{-1} to 622 mSv μC^{-1} for proton energies of 6 and 20 MeV respectively.

Acknowledgements

The authors thank the staffs of Pelletron Linac Accelerator Facility for their constant support during the experiment. Authors sincerely acknowledge Dr. M. Nandy, SINP, Kolkata, India for her guidance regarding the calculation of theoretical neutron yield from different reactions. Authors are grateful to Dr. R.M. Tripathi, Head, Health Physics Division and Dr. K. S. Pradeepkumar, Associate Director, Health, Safety & Environment Group, BARC for the support and inspiration in carrying out these studies.

References

[1] G. Lhersonneau, T. Malkiewicz, M. Fadil, D. Gorelov, P. Jones, P.Z. Ngcobo, J. Sorri, W.H. Trzaska, Neutron yield of thick ^{12}C and ^{13}C targets with 20 and 30 MeV deuterons, Eur. Phys. J. A 52 (2016) 364.

[2] M. Nandy, P.K. Sarkar, T. Sanami, M. Takada, T. Shibata, Neutron emission and dose distribution from natural carbon irradiated with a 12 MeV amu^{-1} $^{12}C^{5+}$ ion beam, J. Radiol. Prot. 36 (2016) 456–473.

[3] T. Kurosawa, T. Nakamura, N. Nakao, T. Shibata, Y. Uwamino, A. Fukumura, Spectral measurements of neutrons, protons, deuterons and tritons produced by 100 MeV/nucleon He bombardment, Nucl. Instrum. Methods Phys. Res. A 430 (1999) 400–422.

[4] T. Kurosawa, N. Nakao, T. Nakamura, Y. Uwamino, T. Shibata, N. Nakanishi, A. Fukumura, K. Murakami, Measurements of secondary neutrons produced from thick targets bombarded by high-energy helium and carbon ions, Nucl. Sci. Eng. 132 (1999) 30–57.

[5] S. Paul, S.P. Tripathy, P.K. Sarkar, Analysis of 3-dimentional track parameters from 2-dimensional images of etched tracks in solid polymeric track detectors, Nucl. Instrum. Methods Phys. Res. A 690 (2012) 58–67.

[6] S. Paul, S.P. Tripathy, G.S. Sahoo, T. Bandyopadhyay, P.K. Sarkar, Measurement of fast neutron spectrum using CR-39 detectors and a new image analysis program (autoTRAK_n), Nucl. Instrum. Methods Phys. Res. A 729 (2013) 444–450.

[7] S.P. Tripathy, S. Paul, G.S. Sahoo, V. Suman, C. Sunil, D.S. Joshi, T. Bandyopadhyay, Measurement of fast neutron spectra from the interaction of 20 MeV protons with thick Be and C targets using CR-39 detector, Nucl. Instrum. Methods Phys. Res. 318 (2014) 237–240.

[8] S. Paul, G.S. Sahoo, S.P. Tripathy, S.C. Sharma, Ramjilal, N.G. Ninawe, C. Sunil, A.K. Gupta, T. Bandyopadhyay, Measurement of neutron spectra generated from bombardment of 4 to 24 MeV protons on a thick ^{9}Be target and estimation of neutron yields, Rev. Sci. Instrum. 85 (2014) 063501.

[9] V. Suman, Sunil C. Nair, S. Paul, K. Biju, G.S. Sahoo, P.K. Sarkar, Thick target double differential neutron energy distribution from ^{12}C + ^{27}Al at 115 MeV, Nucl. Instrum. Methods Phys. Res. Sec. A 800 (2015) 29–33.

[10] T. Kajimoto, N. Shigyo, T. Sanami, Y. Iwamoto, M. Hagiwara, H.S. Lee, A. Soha, E. Ramberg, R. Coleman, D. Jensen, A. Leveling, N.V. Mokhov, D. Boehnlein, K. Vaziri, Y. Sakamoto, K. Ishibashi, H. Nakashima, Measurements and parameterization of neutron energy spectra from targets bombarded with 120 GeV protons, Nucl. Instrum. Methods Phys. Res. Sec. B 337 (2014) 68–77.

[11] V. Suman, S.P. Tripathy, C. Sunil, A.A. Shanbhag, S. Paul, G.S. Sahoo, T. Bandyopadhyay, P.K. Sarkar, Measurement of neutron energy distributions from p + Be reaction at 20 MeV using threshold activation foils, IEEE Trans. Nucl. Sci. 63 (2016) 2283–2292.

[12] A. Wojciechowski, Y.C. Lim, V. Stepanenko, S. Tiutiunnikov, A. Khilmanovich, B. Martsynkevich, A method of measuring the neutron energy spectrum by activation detectors, Measurement 90 (2016) 118–126.

[13] S.P. Tripathy, A.K. Bakshi, V. Sathian, S.M. Tripathi, H.R. Vega-carrillo, M. Nandy, P.K. Sarkar, D.N. Sharma, Measurement of Am–Be spectra (bare and Pb-covered) using TLD pairs in multi-spheres: Spectrum unfolding by different methods, Nucl. Instrum. Methods Phys. Res. A 598 (2009) 556–560.

[14] R. Bedogni, C. Domingo, N. Roberts, D.J. Thomas, M. Chiti, A. Esposito, M.J. Garcia, A. Gentile, Z.Z. Liu, M. De-San-Pedro, Investigation of the neutron spectrum of americium-beryllium sources by bonner sphere spectrometry, Nucl. Instrum. Methods Phys. Res. Sec. A 763 (2014) 547–552.

[15] C. Wernli, H. Hoedlmoser, M. Boschung, E. Hohmann, S. Mayer, Neutron dosimetry around accelerators in Switzerland, Indian J. Pure Appl. Phys. 50 (2012) 757–760.

[16] K. Oda, K. Yoshida, T. Yamauchi, Y. Honda, T. Ikeda, S. Tagawa, Effects of low-LET radiations on CR-39 track detector, Radiat. Meas. 28 (1997) 85–88.

[17] R.L. Fleischer, P.B. Price, R.M. Walker, Nuclear Tracks in Solids, University of Clalifornia Press, Berkeley, CA, 1975.

[18] S.A. Durrani, R.K. Bull, Solid State Nuclear Track Detection, Pergamon Press, Oxford, 1987.

[19] K.K. Dwivedi, S. Ghosh, D. Fink, R. Mishra, S.P. Tripathy, A. Kulshreshtha, D.T. Khating, Modifications in track registration response of PADC detector by energetic protons, Radiat. Meas. 31 (1999) 127–132.

[20] J.F. Ziegler, M.D. Ziegler, J.P. Biersack, SRIM – The stopping and range of ions in matter, Nucl. Instrum. Methods Phys. Res. 268 (2010) 1818–1823.

[21] S. Mayer, M. Boschung, H. Hoedlmoser, Th. Buchillier, C. Bailat, B. Bitterli, Intercomparison of the response of different photon and neutron detectors around a spent fuel cask, Radiat. Meas. 47 (2012) 634–639.

[22] Conversion coefficients for use in radiological protection against external radiation, in: ICRP Publication 74, Ann. ICRP 26 (3–4) (1996).

[23] P.K. Sarkar, T. Bandyaopadhyay, G. Muthukrishnan, S. Ghosh, Neutron production from thick targets bombarded by alpha particles: Experiment and theoretical analysis of neutron energy spectra, Phys. Rev. C 43 (1991) 1855.

[24] O.B. Tarasov, D. Bazin, Development of the program LISE: application to fusion–evaporation, Nucl. Instrum. Methods Phys. Res. 204 (2003) 174–178.

[25] R.G. Thomas Jr., W. Bartolini, Neutron production in Ag, Ta, Au, Pt, and Pb by the interaction of 7.5-14-MeV protons, Phys. Rev. 159 (1967) 1022.

[26] C. Birattari, E. Gadioli, A.M. GrassiStrini, G. Strini, G. Tagliaferri, (p, xn) Reactions induced in ^{169}Tm, ^{181}Ta and ^{209}Bi with 20 to 45 MeV protons, Nucl. Phys. A 166 (1971) 605–623.

[27] G. Chodil, R.C. Jopson, Hans Mark, C.D. Swift, R.G. Thomas, M.K. Yates, (p, n) and (p, 2n) cross sections of nine elements between 7.0 and 15.0 MeV, Nucl. Phys. A 93 (1967) 648–672.

[28] N.N. Krasnov, P.P. Dmitriev, Excitation functions and yields of the reactions $Ta^{181}(d,2n)W^{181}$ and $Ta^{181}(p,n)W^{181}$, At. Energ. 20 (1966) 189–190.

[29] L.F. Hansen, R.C. Jopson, H. Mark, C.D. Swift, $Ta^{181}(p,n)W^{181}$ and $Au^{197}(p,n)Hg^{197}$ excitation functions between 4 and 13 MeV, Nucl. Phys. 30 (1962) 389–398.

[30] V.V. Verbinski, W.R. Burrus, Direct and compound-nucleus neutrons from 14-18-MeV protons on ^{9}Be, ^{14}N, ^{27}Al, ^{56}Fe, ^{115}In, ^{181}Ta, and ^{208}Pb and from 33-MeV Bremsstrahlung on ^{27}Al, ^{206}Pb, ^{208}Pb, and ^{209}Bi, Phys. Rev. 177 (1969) 1671.

[31] R.G. Thomas, W. Bartolini, Neutron Production in Ag, Ta, Au, Pt, and Pb by the interaction of 7.5-14 MeV protons, Phys. Rev. 159 (1967) 1022.